

# Current biased gradiometric flux qubit in a circuit-QED architecture

Mun Dae Kim

College of Liberal Arts, Hongik University, Sejong 30016, Korea

E-mail: mundkim@gmail.com

**Abstract.** We propose a scheme for controlling the gradiometric flux qubit (GFQ) by applying an ac bias current in a circuit-QED architecture. The GFQ is insensitive to the magnetic flux fluctuations, which at the same time makes it challenging to manipulate the qubit states by an external magnetic field. In this study, we demonstrate that an ac bias current applied to the  $\alpha$ -junction of the GFQ can control the qubit states. Further, the present scheme is robust against the charge fluctuation as well as the magnetic flux fluctuations, promising a long coherence time for quantum gate operations. We introduce a circuit-QED architecture to perform the single and two-qubit operations with a sufficiently strong coupling strength.

*Keywords:* gradiometric flux qubit, ac current bias, circuit-QED

## 1. Introduction

Superconducting qubits are promising candidates for noisy intermediate-scale quantum (NISQ) computing due to the scalability and flexibility of circuit design. Unfortunately the electrical and magnetic noises in charge- and phase-based qubits, respectively, are the severe decoherence sources. While the fluctuations of magnetic fluxes in preparing and manipulating the quantum states of the superconducting flux qubits deteriorate the qubit state coherence, for charge qubits the qubit state suffers from the charge fluctuations. The transmon qubit which is coupled with the transmission line resonator at a sweet spot of gate voltage is robust against the charge fluctuations [1]. On the other hand, for phase-based qubit, the gradiometric flux qubit (GFQ) has been intensively investigated because GFQ is robust against the flux fluctuations due to the symmetric design [2, 3, 4, 5, 6, 7].

The simplest three-Josephson junction flux qubit has a fixed gap which depends on the critical current of the so-called  $\alpha$ -junction [8]. The  $\alpha$ -junction has a reduced critical current,  $I_{c,\alpha} = \alpha I_c$ , which can be replaced by a dc-SQUID loop in order to *in situ* adjust the critical current of the  $\alpha$ -junction and thus the qubit energy gap  $\Delta$ . This type of tunable-gap flux qubit, however, is sensitive to the magnetic flux fluctuations responsible for the short decoherence time of qubit operations. On the other hand, the GFQ in Fig. 1 has a symmetric structure so that the magnetic fluxes  $f_1$  and  $f_2$ ,

where  $f_i = \Phi_{\text{ext},i}/\Phi_0$  with the external magnetic flux  $\Phi_{\text{ext},i}$  and the unit flux quantum  $\Phi_0 = h/2e$ , become compensated in the left and right trapping loops, and thus the global magnetic noises cannot affect the qubit states [5]. The GFQ is robust against such global noises that originate from the residual thermal photons in the resonator which is the dominant dephasing source at the symmetric point [10].

However, at the same time, if we apply a magnetic field to manipulate the qubit states, the qubit also does not respond to the operating flux. In order to control the qubit state one should apply a magnetic energy bias which can be induced by generating an asymmetry,  $\epsilon = f_1 - f_2$ , in magnetic fluxes threading into the left and right trapping loop of the GFQ [2, 3, 4, 5], resulting in the deviation of the GFQ state from the symmetric point. This asymmetry then may cause a decoherence to the GFQ states. The  $1/f$  noise from local magnetic defects in the qubit loop may be detrimental to the flux qubit coherence. However, the flux qubit is well protected from the  $1/f$  noise at its symmetric point [9]. In the present study we introduce an ac bias current scheme for operating the GFQ state at the symmetric point, diminishing the decoherence of the GFQ states due to the local defects.

In recently studied schemes an ac bias current is applied to the three-Josephson junction flux qubit to generate a strong coupling between a superconducting qubit and resonator [11, 12, 13, 14, 15, 16, 17], a two-qubit coupling [18, 19], and a resonator-resonator coupling [20, 21, 22]. In those schemes the asymmetry of three-Josephson junction qubit is the origin of the current-qubit coupling. However, this asymmetry may also give rise to the decoherence due to the magnetic flux fluctuations. Hence in this study we introduce an ac current bias scheme for the symmetric GFQ in a circuit-quantum electrodynamics(QED) architecture. The quantized voltage and current modes in the transmission line resonator interact with the qubit coupled to the circuit QED. While charge-based qubits such as transmon are coupled with the voltage modes of the resonator, usually flux qubits are inductively coupled with the current modes through the mutual inductance between the qubit loop and resonator [23, 24]. Previously a GFQ has been coupled to the resonator of circuit-QED architecture via the mutual inductance, providing a weak coupling strength [6].

In this study we provide a scheme for the GFQ biased by an ac current mode of circuit-QED resonator. By obtaining the exact Lagrangian of the system analytically we show that the  $\alpha$ -junction loop of the GFQ can be biased by the ac current,  $I_0$ , in Fig. 1(a) to perform the quantum gate operations. However, the phases,  $\varphi_i (i = 1 \sim 4)$ , of Josephson junctions in the GFQ altogether can not be coupled to the bias current,  $I'_0$ , which means that the GFQ does not respond to the current noises originating from the external charge fluctuations with scale larger than size of the GFQ. The GFQ is insensitive to flux fluctuation, and moreover the ac current biased GFQ is also robust against the charge fluctuations as well, which will guarantee a long coherence time enough for the quantum gate operations. Furthermore, the present ac current bias scheme can induce a sufficiently strong GFQ-resonator coupling to perform the single qubit and two-qubit gate operation in a circuit-QED architecture.

## 2. Ac current biased gradiometric flux qubit

### 2.1. Effective potential for ac bias current coupling

In Fig. 1(a) we introduce an ac current bias scheme for manipulating the GFQ state consisting of left and right trapping loops and  $\alpha$ -junction loop with threading magnetic fluxes,  $\Phi_{\text{ext},i}$  and  $\Phi_{\text{ext},\alpha}$ , respectively. Here we consider that an ac bias current  $I_0$  is applied to the  $\alpha$ -junction loop. In order to obtain the effective potential describing the dynamics of the system, we consider periodic boundary conditions originating from the usual fluxoid quantization condition of superconducting loop [25, 26]. In the system of Fig. 1(a) we have three independent loops whose boundary conditions can be given by

$$-k_1 l - k'_1 l' - k\tilde{l} - \varphi_1 - \varphi_3 - \varphi_4 = 2\pi(n_1 + f_1 + f_{1,\text{ind}}) \quad (1)$$

$$k_2 l + k'_2 l' + k\tilde{l} + \varphi_2 + \varphi_3 + \varphi_4 = 2\pi(n_2 + f_2 + f_{2,\text{ind}}) \quad (2)$$

$$k_1 l - k_2 l + \varphi_1 - \varphi_2 = 2\pi(n + f_\alpha + f_{\alpha,\text{ind}}), \quad (3)$$

where  $k_i$ ,  $\tilde{l}$ ,  $l'$  and  $l$  are the wave vector of the Cooper pairs, the lengths of the central branch, the left(right) branch, and half the length of the dc-SQUID loop, respectively. Here,  $\varphi_i$ 's are the phase differences of the Cooper pair wave function across the Josephson junction,  $f_{1(2),\text{ind}}$  and  $f_{\alpha,\text{ind}}$  are the induced magnetic fluxes of the left(right) trapping loop and the dc-SQUID loop, and  $n_i$ 's are integer. Here, the dc-SQUID loop has the role of the  $\alpha$ -junction loop which provides the tunable qubit energy gap  $\Delta(f_\alpha)$ .

The induced fluxes,  $f_{\text{ind},i} = \Phi_{\text{ind},i}/\Phi_0$ , are given by  $f_{\text{ind},1} = (1/\Phi_0)(-L_g I_1 - \tilde{L}_g I - L'_g I'_1 - L_M I_2 - L'_M I'_2)$ ,  $f_{\text{ind},2} = (1/\Phi_0)(L_g I_2 + \tilde{L}_g I + L'_g I'_2 + L_M I_1 + L'_M I'_1)$ , and  $f_{\text{ind},\alpha} = (1/\Phi_0)(L_g I_1 - L_g I_2)$ . Here, the Cooper pair current  $I_i$  is represented by  $I_i = -(n_c A q_c / m_c) \hbar k_i$  with the Cooper pair density  $n_c$ , the cross section  $A$  of the loop,  $q_c = 2e$  and  $m_c = 2m_e$ . The induced flux,  $\Phi_{\text{ind},1}$ , in the left trapping loop, for example, consists of contributions from the geometric self inductances  $L'_g$ ,  $\tilde{L}_g$  and  $L_g$  of the left branch, the central branch and the left half of the SQUID loop, respectively, and the geometric mutual inductances  $L_M$  and  $L'_M$  between the left trapping loop and the right half of the SQUID loop and the right branch, respectively. For the induced flux,  $f_{\text{ind},\alpha}$ , of  $\alpha$ -junction loop the contributions of mutual inductances between the  $\alpha$ -junction loop and the left and right trapping loops are cancelled, considering the current directions in Figs. 1(b) and (c).

We also introduce the kinetic inductances  $L_K = m_c l / A n_c q_c^2$ ,  $L'_K = m_c l' / A n_c q_c^2$ , and  $\tilde{L}_K = m_c \tilde{l} / A n_c q_c^2$ , [27, 28, 29] and then the induced fluxes become  $f_{\text{ind},1} = [(L'_g/L'_K)(l'/2\pi)k'_1 + (L_g/L_K)(l/2\pi)k_1 + (\tilde{L}_g/\tilde{L}_K)(\tilde{l}/2\pi)k + (L'_M/L'_K)(l'/2\pi)k'_2 + (L_M/L_K)(l/2\pi)k_2]$ ,  $f_{\text{ind},2} = -[(L'_g/L'_K)(l'/2\pi)k'_2 + (L_g/L_K)(l/2\pi)k_2 + (\tilde{L}_g/\tilde{L}_K)(\tilde{l}/2\pi)k + (L'_M/L'_K)(l'/2\pi)k'_1 + (L_M/L_K)(l/2\pi)k_1]$ , and  $f_{\text{ind},\alpha} = -(L_g/L_K)(l/2\pi)(k_1 - k_2)$  to represent the boundary conditions as

$$-\left(1 + \frac{L_g}{L_K}\right)k_1 l - \left(1 + \frac{L'_g}{L'_K}\right)k'_1 l' - \left(1 + \frac{\tilde{L}_g}{\tilde{L}_K}\right)k\tilde{l} - \frac{L'_M}{L'_K}k'_2 l' - \frac{L_M}{L_K}k_2 l = 2\pi\left(n_1 + f_1 + \frac{\varphi_1 + \varphi_3 + \varphi_4}{2\pi}\right) \quad (4)$$

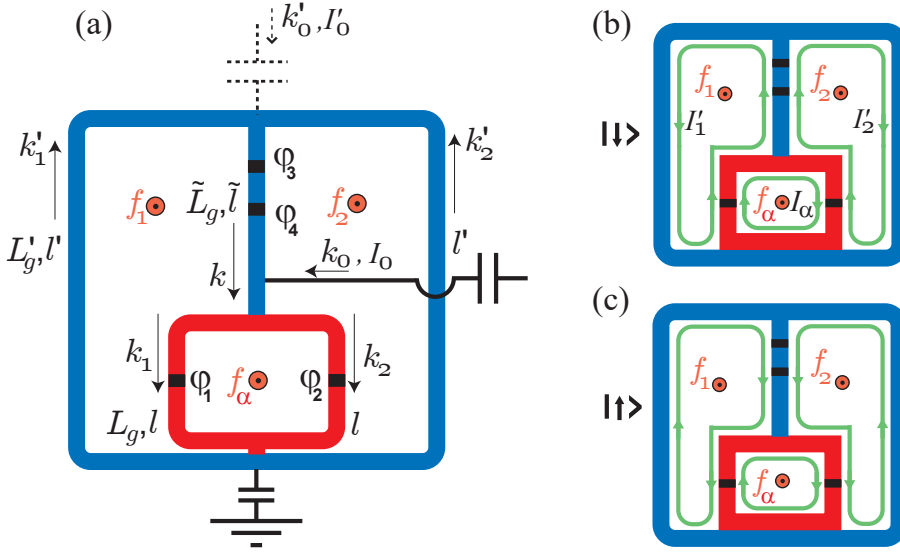


**Figure 1.** (a) A scheme of gradiometric flux qubit with an ac bias current  $I_0$  which can control the qubit state while the ac bias current  $I'_0$  through the dotted line in the figure cannot affect the qubit state. The central dc-SQUID takes the role of the  $\alpha$ -junction loop which provides tunable qubit energy gap  $\Delta(f_\alpha)$ . (b) and (c) show the currents of the qubit states  $|\downarrow\rangle$  and  $|\uparrow\rangle$ , respectively, where the directions of the trapping loop currents are opposite with each other.

$$\left(1 + \frac{L_g}{L_K}\right) k_2 l + \left(1 + \frac{L'_g}{L'_K}\right) k'_2 l' + \left(1 + \frac{\tilde{L}_g}{\tilde{L}_K}\right) k \tilde{l} + \frac{L'_M}{L'_K} k'_1 l' + \frac{L_M}{L_K} k_1 l = 2\pi \left(n_2 + f_2 - \frac{\varphi_2 + \varphi_3 + \varphi_4}{2\pi}\right) \quad (5)$$

$$\left(1 + \frac{L_g}{L_K}\right) (k_1 - k_2) l = 2\pi \left(n + f_\alpha - \frac{\varphi_1 - \varphi_2}{2\pi}\right). \quad (6)$$

If we assume that the GFQ loops and bias line have the same cross section  $A$  and Cooper pair density  $n_c$ , the current conservation conditions at the nodes of the circuit can be represented as

$$k = k'_1 + k'_2, \quad k + k_0 = k_1 + k_2. \quad (7)$$

From the boundary conditions in Eqs. (4), (5) and (6) in conjunction with Eq. (7) we can obtain the wave vectors,  $k_i$ , as follows:

$$k_{1,2} = \frac{2\pi L_K}{l} \left[ \frac{1}{2L_{\text{eff}}} \left( m + f_2 - f_1 - \frac{\varphi_1 + \varphi_2 + 2\varphi_3 + 2\varphi_4}{2\pi} \right) \pm \frac{1}{2(L_K + L_g)} \left( n + f_\alpha - \frac{\varphi_1 - \varphi_2}{2\pi} \right) \right] + \frac{L'_K + L'_g + 2(\tilde{L}_K + \tilde{L}_g) + L'_M}{2L_{\text{eff}}} k_0 \quad (8)$$

$$k'_{1,2} = \frac{2\pi L'_K}{l'} \left[ \frac{1}{2L_{\text{eff}}} \left( m + f_2 - f_1 - \frac{\varphi_1 + \varphi_2 + 2\varphi_3 + 2\varphi_4}{2\pi} \right) \mp \frac{m' + f_1 + f_2 + (1 - \frac{L_M}{L_K + L_g}) f_\alpha}{2(L'_K + L'_g)} \right] - \frac{L_K + L_g + L_M}{2L_{\text{eff}}} k_0 \quad (9)$$

$$k = \frac{2\pi \tilde{L}_K}{\tilde{l} L_{\text{eff}}} \left( m + f_2 - f_1 - \frac{\varphi_1 + \varphi_2 + 2\varphi_3 + 2\varphi_4}{2\pi} \right) - \frac{L_K + L_g + L_M}{L_{\text{eff}}} k_0 \quad (10)$$

with  $L_{\text{eff}} \equiv L_K + L_g + L'_K + L'_g + 2(\tilde{L}_K + \tilde{L}_g) + L_M + L'_M$ ,  $m = n_2 - n_1$  and  $m' = n_1 + n_2$ .

By using the voltage-phase relation  $V = -(\Phi_0/2\pi)\dot{\phi}$  the current relation for Josephson junction in the capacitively-shunted model is written as  $I = -I_c \sin \phi + C\dot{V} = -I_c \sin \phi - C(\Phi_0/2\pi)\ddot{\phi}$ , where  $I_c$  is the critical current and  $C$  the capacitance of Josephson junction. The quantum Kirchhoff relation then is represented as  $-(\Phi_0^2/2\pi L_K)(l/2\pi)k_i = -E_J \sin \phi_i - C(\Phi_0/2\pi)^2\ddot{\phi}_i$  with the Josephson coupling energy  $E_J = \Phi_0 I_c/2\pi$  and the current  $I = -(n_c A q_c/m_c)\hbar k$ . The equation of motion of the phase variables of a Josephson junction,  $C_i(\Phi_0/2\pi)^2\ddot{\phi}_i = -\partial U_{\text{eff}}/\partial \phi_i$ , can be derived from the Lagrange equation  $(d/dt)\partial \mathcal{L}/\partial \dot{\phi}_i - \partial \mathcal{L}/\partial \phi_i = 0$  with the Lagrangian  $\mathcal{L} = \sum_i (1/2)C_i(\Phi_0/2\pi)^2\dot{\phi}_i^2 - U_{\text{eff}}(\{\phi_i\})$  and the effective potential of the system  $U_{\text{eff}}(\{\phi_i\})$ . By using this equation of motion the quantum Kirchhoff relation becomes

$$\frac{\Phi_0^2}{2\pi L_K} \frac{l}{2\pi} k_i - E_J \sin \phi_i = -\frac{\partial U_{\text{eff}}}{\partial \phi_i} \quad (11)$$

from which we can find the effective potential  $U_{\text{eff}}(\{\phi_i\})$  satisfying the quantum Kirchhoff relation as

$$U_{\text{eff}}(\{\phi_i\}) = \frac{\Phi_0^2}{4L_{\text{eff}}} \left( m + f_2 - f_1 - \frac{\varphi_1 + \varphi_2 + 2\varphi_3 + 2\varphi_4}{2\pi} \right)^2 + \frac{\Phi_0^2}{4(L_K + L_g)} \left( n + f_\alpha - \frac{\varphi_1 - \varphi_2}{2\pi} \right)^2 \quad (12)$$

$$- \sum_{i=1}^4 E_{J_i} \cos \varphi_i + \frac{\Phi_0 I_0}{4\pi L_{\text{eff}}} [(L'_K + L'_g + 2\tilde{L}_K + 2\tilde{L}_g + L'_M)(\varphi_1 + \varphi_2) - 2(L_K + L_g + L_M)(\varphi_3 + \varphi_4)].$$

Here the first and second terms correspond to the inductive energy of the trapping loops and the  $\alpha$ -junction loop, the third term the Josephson junction energies, and the last term the coupling energy between the bias current and the phases.

Here, we introduce a coordinate transformation,  $\varphi_{p,m} = (\varphi_1 \pm \varphi_2)/2$  and  $\tilde{\varphi}_{p,m} = (\varphi_3 \pm \varphi_4)/2$ , to represent the effective potential as

$$U_{\text{eff}}(\varphi_{p,m}, \tilde{\varphi}_{p,m}) = \frac{\Phi_0^2}{4L_{\text{eff}}} \left( m + f_2 - f_1 - \frac{2\varphi_p + 4\tilde{\varphi}_p}{2\pi} \right)^2 + \frac{\Phi_0^2}{4(L_K + L_g)} \left( n + f_\alpha - \frac{\varphi_m}{\pi} \right)^2$$

$$- 2E_J \cos \varphi_p \cos \varphi_m - 2\tilde{E}_J \cos \tilde{\varphi}_p \cos \tilde{\varphi}_m \quad (13)$$

$$+ \frac{\Phi_0 I_0}{2\pi L_{\text{eff}}} [(L'_K + L'_g + 2\tilde{L}_K + 2\tilde{L}_g + L'_M)\varphi_p - 2(L_K + L_g + L_M)\tilde{\varphi}_p],$$

where we set  $E_{J1} = E_{J2} = E_J$  and  $E_{J3} = E_{J4} = \tilde{E}_J$ . In Fig. 2(a) we show the effective potential  $U_{\text{eff}}(\varphi_{p,m}, \tilde{\varphi}_{p,m})$  as a function of  $\varphi_p$  and  $\tilde{\varphi}_m$  for  $I_0 = 0$ . The value of  $\varphi_m$  and  $\tilde{\varphi}_p$  are determined by numerically minimizing the effective potential  $U_{\text{eff}}(\varphi_{p,m}, \tilde{\varphi}_{p,m})$ . Actually we have found that for different even-odd parity of  $m$  and  $n$  the local minima connected by the dotted line in Fig. 2(a) can be formed with the double well structure as shown in Fig. 2(b). Here we set  $m = 0$ ,  $n = 1$ ,  $f_\alpha = 0.2$ ,  $\tilde{E}_J/E_J = 2.0$ , and further  $f_1 = f_2$  so the external fluxes,  $f_1$  and  $f_2$ , do not affect the qubit states.

At the two local minima denoted as  $|\uparrow\rangle$  and  $|\downarrow\rangle$  in Fig. 2(a) we found that the inductive energy,  $U_{\text{ind}}$ , of the first two terms in the effective potential of Eq. (13) is  $U_{\text{ind}}/E_J \sim 0.006$ , while the Josephson junction energy,  $U_{\text{JJ}}$ , of third and fourth terms  $U_{\text{JJ}}/E_J \sim -2.886$ . Hence, for simplicity, we can neglect the induced energies in the

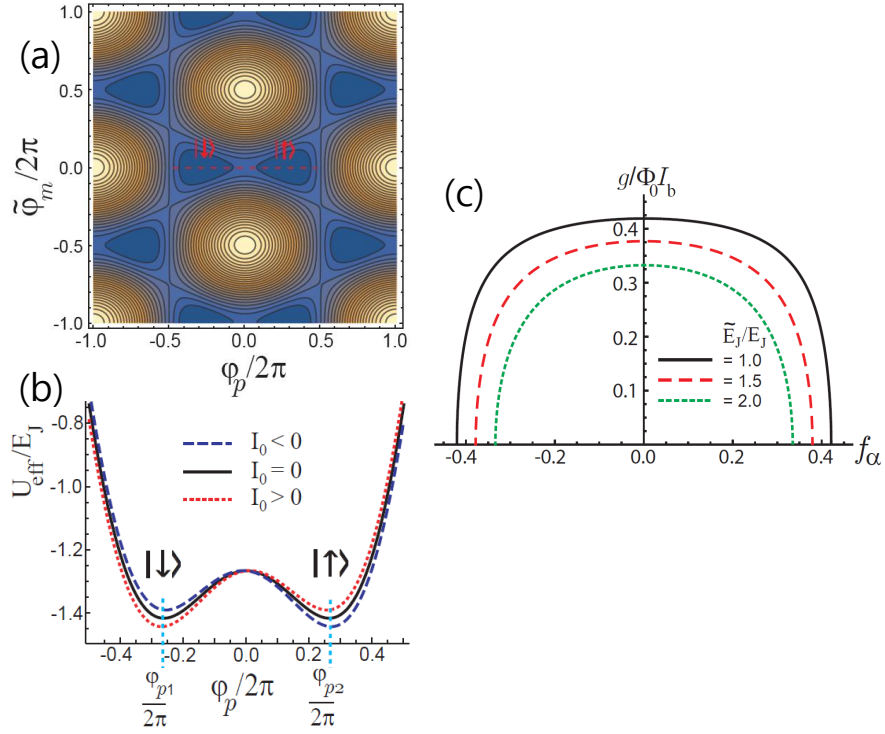


**Figure 2.** (a) Numerical contour plot for the effective potential in Eq. (13) for  $I_0 = 0$ . The states at two local minima are denoted as  $|\downarrow\rangle$  and  $|\uparrow\rangle$ . Here we set  $f_\alpha = 0.2$ ,  $\tilde{E}_J/E_J = 2.0$ , and  $f_1 = f_2$ . (b) Double well potential along the dotted line in (a). For finite bias current  $I_0$  the potential becomes tilted in opposite directions depending on the sign of  $I_0$ . (c) Coupling strength  $g$  between the GFQ and the bias current with amplitude  $I_b$ .

effective potentials of Eqs. (12) and (13). Actually in experimental situations the geometric inductance is dominant over the kinetic inductance,  $L_g \gg L_K$ , and the inductive energy  $\Phi_0^2/L_g \sim O(10^3 E_J)$  [34] is much larger than the Josephson energy scale  $E_J$ , which means that the following boundary conditions should be satisfied,

$$n + f_\alpha - \frac{\varphi_1 - \varphi_2}{2\pi} \approx 0, \quad (14)$$

$$m + f_2 - f_1 - \frac{\varphi_1 + \varphi_2 + 2\varphi_3 + 2\varphi_4}{2\pi} \approx 0, \quad (15)$$

in order to neglect the first two terms of  $U_{\text{eff}}(\{\phi_i\})$  in Eq. (12) in spite of the large values of  $\Phi_0^2/4L_{\text{eff}}E_J$  and  $\Phi_0^2/4(L_K + L_g)E_J$ . Here, we set  $\Phi_0^2/4L_{\text{eff}}E_J = 1000$  and  $\Phi_0^2/4(L_K + L_g)E_J = 3000$ . The boundary condition of Eq. (14) can also be obtained from Eq. (3) because in the parameter regime for flux qubits the phase evolution,  $kl$ , of Cooper pair wave function and the induced magnetic flux,  $f_{\alpha, \text{ind}}$ , are negligible compared to the phase difference  $\varphi$  across the Josephson junction. In the same way the boundary condition of Eq. (15) can also be obtained by subtracting two boundary conditions of Eqs. (1) and (2).

We can represent the boundary conditions in Eqs. (14) and (15) in the transformed coordinate as  $n + f_\alpha - \varphi_m/\pi \approx 0$  and  $m + f_2 - f_1 - (2\varphi_p + 4\tilde{\varphi}_p)/2\pi \approx 0$ , and thus the

last term of Eq. (13) can be written as

$$\begin{aligned} & \frac{\Phi_0 I_0}{2\pi L_{\text{eff}}} [(L'_K + L'_g + 2\tilde{L}_K + 2\tilde{L}_g + L'_M)\varphi_p + (L_K + L_g + L_M)(\varphi_p - \pi(m + f_2 - f_1))] \\ &= \frac{\Phi_0 I_0}{2\pi} \left[ \varphi_p - \frac{(L_K + L_g + L_M)\pi}{L_{\text{eff}}} (m + f_2 - f_1) \right]. \end{aligned} \quad (16)$$

The effective potential  $U_{\text{eff}}(\varphi_{p,m}, \tilde{\varphi}_{p,m})$  in Eq. (13) then can be approximated to a function of  $\varphi_p$  and  $\tilde{\varphi}_m$ ,  $V(\varphi_p, \tilde{\varphi}_m)$ , apart from the constant term:

$$V(\varphi_p, \tilde{\varphi}_m) = -2E_J \cos \pi(n + f_\alpha) \cos \varphi_p - 2\tilde{E}_J \cos \frac{\pi(m + f_2 - f_1) - \varphi_p}{2} \cos \tilde{\varphi}_m + \frac{\Phi_0 I_0}{2\pi} \varphi_p, \quad (17)$$

which shows that the GFQ can be coupled to the ac bias current through only the phase,  $\varphi_\alpha$ , of Josephson junctions in the  $\alpha$ -junction loop with the strength independent of the values of individual inductances. Alternatively, with the boundary condition of Eq. (15) the coupling between the bias current and phase can also be represented in terms of  $\tilde{\varphi}_p$ .

On the contrary, the phases,  $\varphi_i (i = 1 \sim 4)$ , of Josephson junctions in the GFQ altogether cannot be coupled to the bias current. Until now we have considered the bias current  $I_0$  in Fig. 1(a). However, we can also apply the bias current  $I'_0 = -(n_c A q_c / m_c) \hbar k'_0$ , denoted as dotted line in Fig. 1(a), at the node that the wave vectors  $k, k'_1$  and  $k'_2$  meet. Instead of the boundary conditions in Eq. (7) in this case we have the conditions  $k'_1 + k'_2 + k'_0 = k$  and  $k = k_1 + k_2$ . Through a similar derivation to the previous one for Fig. 1(a) with above conditions in conjunction with Eqs. (1)-(3) we can obtain the effective potential

$$\begin{aligned} U_{\text{eff}}(\{\phi_i\}) &= \frac{\Phi_0^2}{4L_{\text{eff}}} \left( m + f_2 - f_1 - \frac{\varphi_1 + \varphi_2 + 2\varphi_3 + 2\varphi_4}{2\pi} \right)^2 + \frac{\Phi_0^2}{4(L_K + L_g)} \left( n + f_\alpha - \frac{\varphi_1 - \varphi_2}{2\pi} \right)^2 \\ &\quad - \sum_{i=1}^4 E_{J_i} \cos \varphi_i + \frac{\Phi_0 I'_0 (L'_K + L'_g + L'_M)}{4\pi L_{\text{eff}}} (\varphi_1 + \varphi_2 + 2\varphi_3 + 2\varphi_4), \end{aligned} \quad (18)$$

where the last term describing the coupling to the bias current  $I'_0$  has a form different from that in Eq. (12).

Similarly to the previous case we also have the boundary condition,  $(\varphi_1 + \varphi_2 + 2\varphi_3 + 2\varphi_4)/2\pi \approx m + f_2 - f_1$ . The last term of Eq. (18) then becomes a constant term,  $[\Phi_0 I'_0 (L'_K + L'_g + L'_M)/2L_{\text{eff}}](m + f_2 - f_1)$ , which means that with this scheme the bias-current cannot be coupled with the phases of the Josephson junctions of the GFQ and thus we cannot control the qubit state in contrast to the previous scheme in Fig. 1(a). Further, the charge fluctuations with scale larger than size of the GFQ can be considered to induce noisy bias currents through the dotted line in Fig. 1(a) which, however, cannot affect the qubit state. Hence the present ac bias current scheme for the GFQ is robust against the charge fluctuations as well as the magnetic flux fluctuations, which may provide a long coherence time for the NISQ computing.

In Fig. 1(a) the bias current line needs an airbridge structure which is not so simple to construct. Many experimental efforts have been devoted to mitigate the additional loss to be small [30, 31], and moreover the undesired effect of airbridge capacitance has also been studied to be kept at a minimum level [32]. However, through the small

capacitance a residual current,  $\tilde{I} = -(n_c A q_c / m_c) \hbar \tilde{k}$  with the Cooper pair wave vector  $\tilde{k}$ , may flow into the branch line. The current conservation conditions then become  $k'_1 + k'_2 + \tilde{k} = k$  and  $k = k_1 + k_2$ , which are the same as those conditions above Eq. (18) for the current  $I'_0 = -(n_c A q_c / m_c) \hbar k'_0$ , and thus gives rise to the same constant coupling term as the last term of Eq. (18). Hence, the GFQ state will be also robust against the fluctuations due to the residual current  $\tilde{I}$  through the airbridge.

## 2.2. Coupling strength between GFQ and ac bias current

The effective potential in Eq. (17) for  $I_0 = 0$  with  $m = 0$ ,  $n = 1$  and  $f_1 = f_2$  becomes  $V(\varphi_p, \tilde{\varphi}_m) = 2E_J \cos(\pi f_\alpha) \cos \varphi_p - 2\tilde{E}_J \cos(\varphi_p/2) \cos \tilde{\varphi}_m$ . Here we can obtain analytically the position of local minima,  $(\varphi_{p1}, \tilde{\varphi}_{m1})$  and  $(\varphi_{p2}, \tilde{\varphi}_{m2})$ , corresponding to the states  $|\downarrow\rangle$  and  $|\uparrow\rangle$  with energy levels  $E_\downarrow$  and  $E_\uparrow$ , respectively, which are symmetric with respect to  $\varphi_p = 0$  as shown in Fig. 2(a). From  $\partial V(\varphi_p, \tilde{\varphi}_m) / \partial \tilde{\varphi}_m = 2\tilde{E}_J \cos(\varphi_p/2) \sin \tilde{\varphi}_m = 0$  and  $\partial V(\varphi_p, \tilde{\varphi}_m) / \partial \varphi_p = -2E_J \cos \pi f_\alpha \sin \varphi_p + \tilde{E}_J \cos \tilde{\varphi}_m \sin(\varphi_p/2) = 0$  we have

$$\tilde{\varphi}_{m,i} = 0 \quad \text{and} \quad \cos\left(\frac{\varphi_{p,i}}{2}\right) = \frac{\tilde{E}_J}{4E_J \cos(\pi f_\alpha)} \quad (19)$$

with  $i = 1, 2$ . The trapping loop currents of qubit states,  $|\downarrow\rangle$  and  $|\uparrow\rangle$ , are shown in Figs. 1 (b) and (c), where they are in opposite directions with each other while the directions of  $\alpha$ -junction loop are the same. In the qubit state  $|\uparrow\rangle(|\downarrow\rangle)$ , we calculate the trapping loop current  $I'_i = -(n_c A q_c / m_c) \hbar k'_i$  with  $k'_i$  in Eq. (9). Since  $(n_c A q_c / m_c) \hbar (2\pi L'_k / l') = \Phi_0$ , we can calculate numerically the reduced dimensionless current as  $I'_1 L_{\text{eff}} / \Phi_0 = I'_2 L_{\text{eff}} / \Phi_0 = \pm 0.00123$  for  $f_1 = f_2 = 0.94$ ,  $L_M / (L_k + L_g) = 0.4$ ,  $f_\alpha = 0.2$  and  $\tilde{E}_J / E_J = 2.0$  with  $m = 0$ ,  $n = 1$  and  $m' = -2$ . Here the integer  $m'$  is determined by minimizing the potential energy ( see the details in appendix A). The  $\alpha$ -junction loop current is given by  $I_\alpha = (I_1 - I_2) / 2$  with  $I_i = -(2\pi E_J / \Phi_0) \sin \varphi_i$  and thus  $I_i L_{\text{eff}} / \Phi_0 = -(\pi/2)(4L_{\text{eff}} E_J / \Phi_0^2) \sin \varphi_i$ . For the parameter value of  $\Phi_0^2 / 4L_{\text{eff}} E_J = 1000$  with  $L_{\text{eff}} = 15\text{pH}$  and  $E_J / h = 200\text{GHz}$  we obtain  $I_\alpha L_{\text{eff}} / \Phi_0 = 0.00022$ , i. e.,  $|I'_i| = 170\text{nA}$  and  $I_\alpha = 30\text{nA}$ .

The qubit energy gap  $\Delta$  of the GFQ can be controlled by the ratio  $\tilde{E}_J / E_J$  as well as the magnetic flux  $f_\alpha$  threading the  $\alpha$ -junction loop. We calculate numerically the qubit energy gap  $\Delta = 2t_q$  with  $t_q$  being the tunnelling amplitude across the one-dimensional potential well in Fig. 2(b) [33]. We can identify the parameter regime for a specific qubit energy gap  $\Delta$  with the ratio of the Josephson coupling energy to the charging energy  $E_J / E_C = 40$  [34]. In order to obtain  $\Delta / h \sim 1\text{GHz}$ , for example, we adjust  $f_\alpha = 0.2$  with  $\tilde{E}_J / E_J = 2.0$ . Actually, as  $f_\alpha$  or  $\tilde{E}_J / E_J$  increases, the barrier of double well potential decreases and thus  $\Delta$  increases.

For  $I_0 \neq 0$  the effective potential  $V(\varphi_p, \tilde{\varphi}_m) = 2E_J \cos(\pi f_\alpha) \cos \varphi_p - 2\tilde{E}_J \cos(\varphi_p/2) \cos \tilde{\varphi}_m + (\Phi_0 I_0 / 2\pi) \varphi_p$  becomes tilted as shown in Fig. 2(b). The energy levels can be represented as  $(E_\downarrow - \Phi_0 I_0 \alpha / 2\pi) |\downarrow\rangle \langle \downarrow| + (E_\uparrow + \Phi_0 I_0 \alpha / 2\pi) |\uparrow\rangle \langle \uparrow|$ , and



thus the tight binding Hamiltonian can be written as

$$H = E_{\downarrow} |\downarrow\rangle\langle\downarrow| + E_{\uparrow} |\uparrow\rangle\langle\uparrow| - t_q (|\downarrow\rangle\langle\uparrow| + |\uparrow\rangle\langle\downarrow|) - \frac{\Phi_0 I_0}{2\pi} \alpha (|\downarrow\rangle\langle\downarrow| - |\uparrow\rangle\langle\uparrow|), \quad (20)$$

where from Eq. (19)  $\alpha = |\varphi_{p1}| = |\varphi_{p2}|$  is given by

$$\alpha = 2 \cos^{-1} \left( \frac{\tilde{E}_J}{4E_J \cos(\pi f_{\alpha})} \right). \quad (21)$$

Here we consider that an ac bias current  $I_0 = -I_b \sin \omega t$  is applied, and introduce a coordinate transformation such as  $|0\rangle = (|\downarrow\rangle + |\uparrow\rangle)/\sqrt{2}$  and  $|1\rangle = (|\downarrow\rangle - |\uparrow\rangle)/\sqrt{2}$ . For the degenerate case,  $E_{\downarrow} = E_{\uparrow}$ , the Hamiltonian in Eq. (20) can be transformed to  $\mathcal{H} = (\Delta/2)\sigma_z + g \sin \omega t \sigma_x$  in the basis of  $\{|0\rangle, |1\rangle\}$ . The coupling constant  $g = (\Phi_0 I_b / 2\pi) \alpha$  also depends on  $\tilde{E}_J / E_J$  and  $f_{\alpha}$  such that

$$g = \frac{\Phi_0 I_b}{\pi} \cos^{-1} \left( \frac{\tilde{E}_J}{4E_J \cos(\pi f_{\alpha})} \right). \quad (22)$$

In Fig. 2(c) we show the coupling strength  $g$  as a function of  $f_{\alpha}$  for several values of  $\tilde{E}_J / E_J$ . In this study we set  $\tilde{E}_J / E_J = 2.0$  and  $f_{\alpha} = 0.2$  so that  $g / \Phi_0 I_b \approx 0.3$ .

### 3. Circuit QED with gradiometric flux qubits

In Fig. 3(a) we present a scheme for the GFQ in a circuit-QED architecture, where a GFQ is coupled with the resonator through a large capacitance with width  $d$ . The state of transmission line resonator of the circuit-QED architecture can be described in

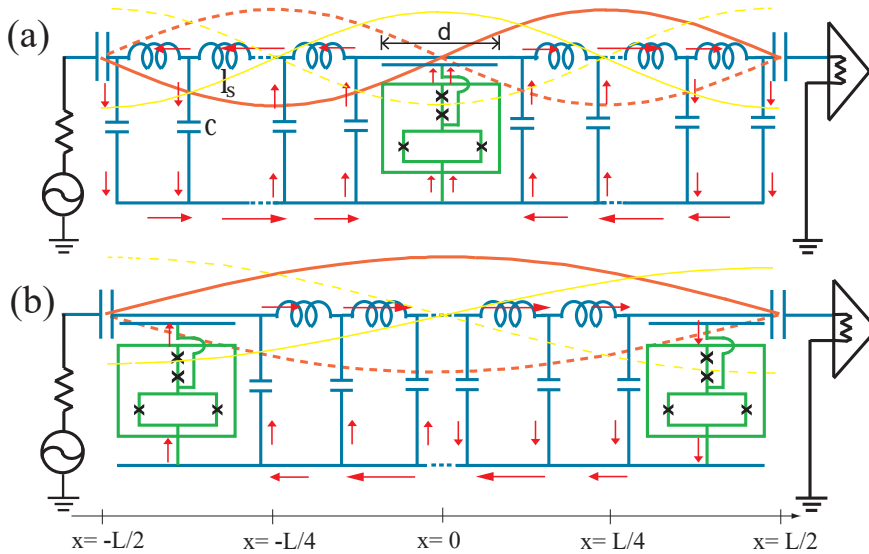


**Figure 3.** (a) A GFQ coupled with an current mode (orange) and a voltage mode (yellow) of the transmission line resonator of the circuit-QED architecture through a large capacitance with width  $d$ , where arrows show the current directions and amplitudes. (b) Two GFQs at the ends of the resonator are coupled with each other through the current mode of resonator.

terms of the electric potential and current modes. The Lagrangian of the resonators is represented as  $\mathcal{L}(\theta, \dot{\theta}; t) = \int_{-L/2}^{L/2} [(l_s/2)\partial_t^2\theta(x, t) - (1/2c)\partial_x^2\theta(x, t)] dx$ , where  $l_s$  and  $c$  are the inductance and the capacitance per unit length of the uniform transmission line resonator, respectively, and  $\theta(x, t) = \int_{-L/2}^x dx' Q(x', t)$  with the linear charge density  $Q(x, t)$  [35]. As shown in Fig. 3(a) the charge neutrality imposes the boundary condition,  $\theta(-L/2, t) = \theta(L/2, t) = 0$ , which allows the normal mode expansion such as  $\theta(x, t) = \sqrt{\frac{2}{L}} \sum_n \left( q_{2n-1}(t) \cos \frac{(2n-1)\pi x}{L} + q_{2n}(t) \sin \frac{2n\pi x}{L} \right)$  with a positive integer  $n$ . Here, the electric potential can be represented as  $V(x, t) = (1/c)\partial\theta(x, t)/\partial x$  and the current  $I(x, t) = \partial\theta(x, t)/\partial t$ . The Hamiltonian, then, can be derived from the Lagrangian as  $\mathcal{H} = \sum_n [(l_s/2)\dot{q}_n^2 + (1/2c)(n\pi/L)^2 q_n^2]$  which can be diagonalized as  $\mathcal{H} = \sum_n \hbar\omega_n (a_n^\dagger a_n + 1/2)$  with the representation  $\hat{q}_n(t) = \sqrt{\hbar\omega_n c/2}(L/n\pi)(a_n(t) + a_n^\dagger(t))$ ,  $\hat{p}_n(t) = -i\sqrt{\hbar\omega_n l_s/2}(a_n(t) - a_n^\dagger(t))$  and  $p_n = l_s \dot{q}_n$ . Here,  $a_n^\dagger$  and  $a_n$  are bosonic operators satisfying  $[a_m, a_n^\dagger] = \delta_{m,n}$  and  $\omega_n = n\pi v/L$  with  $v = 1/\sqrt{l_s c}$ .

In Fig. 3(a) the current mode displayed as orange line can be obtained by  $I(x, t) = \partial\theta(x, t)/\partial t$  for  $n = 2$  as

$$\hat{I}_2(x, t) = -i\sqrt{\frac{\hbar\omega_2}{l_s L}} \sin \frac{2\pi x}{L} (a_2(t) - a_2^\dagger(t)). \quad (23)$$

From Eqs. (20) and (23) we can have the Hamiltonian for the combined system of the resonator and the GFQ such as

$$H = \hbar\omega_2 \left( a_2^\dagger a_2 + \frac{1}{2} \right) + E_\downarrow |\downarrow\rangle\langle\downarrow| + E_\uparrow |\uparrow\rangle\langle\uparrow| - t_q (|\downarrow\rangle\langle\uparrow| + |\uparrow\rangle\langle\downarrow|) + ig (|\downarrow\rangle\langle\downarrow| - |\uparrow\rangle\langle\uparrow|) (a_2 - a_2^\dagger). \quad (24)$$

If we assume a constant capacitance  $c$  per unit length in Fig. 3(a), the bias current  $\hat{I}_0 = \int_{-d/2}^{d/2} \hat{q}(x, t) dx$  with  $\hat{q}(x, t) = \partial\hat{I}_2(x, t)/\partial x$  can be represented as  $\hat{I}_0 = \hat{I}_2(d/2, t) - \hat{I}_2(-d/2, t) = -2i\sqrt{\hbar\omega_2/l_s L} \sin(\pi d/L) (a_2(t) - a_2^\dagger(t))$ , and thus the amplitude  $I_b$  of the bias current is given by  $I_b = 2\sqrt{\hbar\omega_2/l_s L} \sin(\pi d/L)$  which has a finite value for  $d \neq 0$ . In fact, however, the capacitance density should be larger around the large capacitor. This general situation has been considered to calculate the bias current amplitude  $I_b = \sqrt{\hbar\omega_2/l_s L} \delta$  with a parameter  $\delta$  depending on the parameters of capacitor between the qubit and resonator [16]. The coupling strength  $g$ , then, is given by  $g = \alpha(\Phi_0/2\pi)\delta\sqrt{(\hbar\omega_2/l_s L)}$  with  $\alpha$  in Eq. (21), where the coupling strength can be sufficiently strong,  $g \sim \hbar\omega_1$ , due to the large capacitance between the qubit and resonator. For the degenerate case that  $E_\downarrow = E_\uparrow$  this Hamiltonian can be represented in the basis of  $\{|0\rangle, |1\rangle\}$  as  $\tilde{H} = \hbar\omega_2 a_2^\dagger a_2 + (\Delta/2)\sigma_z + ig\sigma_x (a_2 - a_2^\dagger)$ , and further transformed to  $\tilde{H}_{\text{RWA}} = \hbar\omega_2 a_2^\dagger a_2 + (\Delta/2)\sigma_z - ig(a_2^\dagger \sigma_- - \sigma_+ a_2)$  in the rotating wave approximation.

Two GFQs can be coupled to perform the two-qubit gate operations. As shown in Fig. 3(b) two GFQs are coupled through the current mode,  $I_1(x, t)$  for  $n = 1$ , of the resonator as

$$\hat{I}_1(x, t) = -i\sqrt{\frac{\hbar\omega_1}{l_s L}} \cos \frac{\pi x}{L} (a_1(t) - a_1^\dagger(t)), \quad (25)$$

from which the coupling strength is given by  $g_{l(r)} = \alpha_{l(r)}(\Phi_0/2\pi)\delta\sqrt{(\hbar\omega_1/lL)}$  for left(right) qubit with  $\alpha_{l(r)}$  being  $\alpha$  in Eq. (21). Then the Hamiltonian for two coupled qubits in the dispersive regime,  $\Delta'_j = \Delta_j - \omega_1 \gg g_j$ , is written as [16, 36]

$$\mathcal{H}_{2qubit} = \omega_1 a_1^\dagger a_1 + \sum_{j=l,r} \frac{\tilde{\Delta}_j}{2} \sigma_{z_j} + \frac{1}{2} \left( \frac{1}{\Delta'_l} + \frac{1}{\Delta'_r} \right) g_l g_r (\sigma_{-l} \sigma_{+r} + \sigma_{+l} \sigma_{-r}), \quad (26)$$

where  $\tilde{\Delta}_j = \Delta_j + g_j^2/\Delta'_j$  with  $\Delta_{l(r)}$  being the energy gap for left(right) qubit.

#### 4. Conclusions

The GFQ is insensitive to the magnetic flux fluctuations due to the symmetry of design, but at the same time it is difficult to manipulate the GFQ states by an external magnetic flux. In this study, thus, we introduced a scheme for controlling the GFQ by an ac bias current. By deriving exactly the effective Lagrangian of the system we showed that the phase variables of the  $\alpha$ -junction loop in Fig. 1(a) of the GFQ become coupled with the ac bias current  $I_0$  as in the last term of Eq. (17). However, if we try to couple all phases,  $\varphi_i (i = 1 \sim 4)$ , with  $I'_0$  in Fig. 1(a), the coupling term becomes constant, which means that the GFQ do not respond to the external current  $I'_0$  and thus to the charge fluctuations with the length scale larger than the size of GFQ. Therefore, the present GFQ scheme is robust against charge fluctuations as well as magnetic fluctuations, which ensures a long coherence time for NISQ computing.

Further we obtained an analytic expression for the coupling strength  $g$  between the bias current and the phase variables of the GFQ, which is sufficiently strong for the quantum gate operations. We also introduced a circuit-QED scheme involving the GFQs to provide a scheme for performing the single- and two-qubit operations.

#### Acknowledgments

This research was supported by Basic Science Research Program through the National Research Foundation of Korea(NRF) funded by the Ministry of Education(2019R1I1A1A01061274), 2021 Hongik University Research Fund, and Korea Institute for Advanced Study(KIAS) grant funded by the Korea government.

#### Appendix A. A constant term in effective potential $U_{\text{eff}}$

We consider a GFQ scheme different from that in Fig. 1(a). In Fig. A1 two Josephson junctions with phase differences,  $\varphi'_1$  and  $\varphi'_2$ , in trapping loops are additionally introduced. The boundary conditions then become

$$-k_1 l - k'_1 l' - k\tilde{l} - \varphi_1 - \varphi_3 - \varphi_4 + \varphi'_1 = 2\pi(n_1 + f_1 + f_{1,\text{ind}}) \quad (\text{A.1})$$

$$k_2 l + k'_2 l' + k\tilde{l} + \varphi_2 + \varphi_3 + \varphi_4 - \varphi'_2 = 2\pi(n_2 + f_2 + f_{2,\text{ind}}) \quad (\text{A.2})$$

$$k_1 l - k_2 l + \varphi_1 - \varphi_2 = 2\pi(n + f_\alpha + f_{\alpha,\text{ind}}), \quad (\text{A.3})$$

and with the induced fluxes,  $f_{\text{ind},i} = \Phi_{\text{ind},i}/\Phi_0$ , in the main manuscript these conditions can be represented as

$$-\left(1+\frac{L_g}{L_K}\right)k_1l - \left(1+\frac{L'_g}{L'_K}\right)k'_1l' - \left(1+\frac{\tilde{L}_g}{\tilde{L}_K}\right)k\tilde{l} - \frac{L'_M}{L'_K}k'_2l' - \frac{L_M}{L_K}k_2l = 2\pi\left(n_1+f_1+\frac{\varphi_1+\varphi_3+\varphi_4-\varphi'_1}{2\pi}\right) \quad (\text{A.4})$$

$$\left(1+\frac{L_g}{L_K}\right)k_2l + \left(1+\frac{L'_g}{L'_K}\right)k'_2l' + \left(1+\frac{\tilde{L}_g}{\tilde{L}_K}\right)k\tilde{l} + \frac{L'_M}{L'_K}k'_1l' + \frac{L_M}{L_K}k_1l = 2\pi\left(n_2+f_2-\frac{\varphi_2+\varphi_3+\varphi_4-\varphi'_2}{2\pi}\right) \quad (\text{A.5})$$

$$\left(1+\frac{L_g}{L_K}\right)(k_1-k_2)l = 2\pi\left(n+f_\alpha-\frac{\varphi_1-\varphi_2}{2\pi}\right). \quad (\text{A.6})$$

With the current conservation conditions at nodes,  $k = k'_1 + k'_2$  and  $k = k_1 + k_2$ , we obtain

$$k_{1,2} = \frac{2\pi L_K}{l} \left[ \frac{1}{2L_{\text{eff}}} \left( m + f_2 - f_1 - \frac{\varphi_1 + \varphi_2 + 2\varphi_3 + 2\varphi_4 - \varphi'_1 - \varphi'_2}{2\pi} \right) \pm \frac{1}{2(L_K + L_g)} \left( n + f_\alpha - \frac{\varphi_1 - \varphi_2}{2\pi} \right) \right] \quad (\text{A.7})$$

$$k'_{1,2} = \frac{2\pi L'_K}{l'} \left[ \frac{1}{2L_{\text{eff}}} \left( m + f_2 - f_1 - \frac{\varphi_1 + \varphi_2 + 2\varphi_3 + 2\varphi_4 - \varphi'_1 - \varphi'_2}{2\pi} \right) \mp \frac{1}{2(L'_K + L'_g - L'_M)} \left( m' + f_1 + f_2 + \left( 1 - \frac{L_M}{L_K + L_g} \right) f_\alpha - \frac{\varphi'_1 - \varphi'_2}{2\pi} \right) \right] \quad (\text{A.8})$$

$$k = \frac{2\pi \tilde{L}_K}{\tilde{l} L_{\text{eff}}} \left( m + f_2 - f_1 - \frac{\varphi_1 + \varphi_2 + 2\varphi_3 + 2\varphi_4 - \varphi'_1 - \varphi'_2}{2\pi} \right), \quad (\text{A.9})$$

where  $L_{\text{eff}} = L_K + L_g + L'_K + L'_g + 2(\tilde{L}_K + \tilde{L}_g) + L_M + L'_M$ ,  $m = n_2 - n_1$  and  $m' = n_1 + n_2$ .

In order to satisfy the quantum Kirchhoff relation,  $(\Phi_0^2/2\pi L_K)(l/2\pi)k_i - E_J \sin \phi_i =$

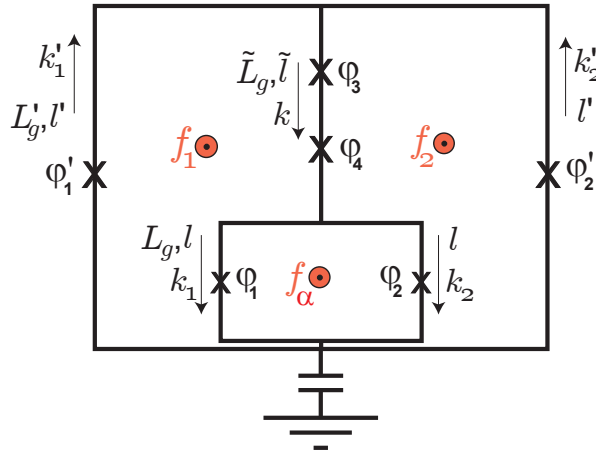


**Figure A1.** Two Josephson junctions with phase differences  $\varphi'_i$  are additionally introduced in the left and right trapping loops of a gradiometric flux qubit.

$-\partial U_{\text{eff}}/\partial \phi_i$ , the effective potential  $U_{\text{eff}}$  should be

$$U_{\text{eff}}(\{\varphi_i, \varphi'_i\}) = \frac{\Phi_0^2}{4L_{\text{eff}}} \left( m + f_2 - f_1 - \frac{\varphi_1 + \varphi_2 + 2\varphi_3 + 2\varphi_4 - \varphi'_1 - \varphi'_2}{2\pi} \right)^2 + \frac{\Phi_0^2}{4(L_K + L_g)} \left( n + f_\alpha - \frac{\varphi_1 - \varphi_2}{2\pi} \right)^2 + \frac{\Phi_0^2}{4(L'_K + L'_g)} \left[ m' + f_1 + f_2 + \left( 1 - \frac{L_M}{L_K + L_g} \right) f_\alpha - \frac{\varphi'_1 - \varphi'_2}{2\pi} \right]^2 - \sum_{i=1}^4 E_{Ji} \cos \varphi_i. \quad (\text{A.10})$$

Here, we consider the limit that  $\varphi'_1$  and  $\varphi'_2$  diminish to zero, which means that virtually there is no effect of the additionally introduced two Josephson junctions. Then the boundary conditions in Eqs. (A.1)-(A.3) reduce to those in Eqs. (1)-(3), but the effective potential in Eq. (A.10) has an additional constant term,

$$\frac{\Phi_0^2}{4(L'_K + L'_g)} \left[ m' + f_1 + f_2 + \left( 1 - \frac{L_M}{L_K + L_g} \right) f_\alpha \right]^2, \quad (\text{A.11})$$

which should have been included in the effective potential in Eq. (12). Actually this constant term cannot be obtained in the effective potential for the GFQ in Fig. 1(a) from the quantum Kirchhoff relation in Eq. (11). But in order to calculate the current  $I'$  with Eq. (9) we need to minimize this term to determine the value of integer  $m'$ .

## References

- [1] Koch J, Yu T M, Gambetta J, Houck A A, Schuster D I, Majer J, Blais A, Devoret M H, Girvin S M and Schoelkopf R J 2007 Charge-insensitive qubit design derived from the Cooper pair box *Phys. Rev. A* **76** 042319
- [2] Paauw F G, Fedorov A, Harmans C J P M and Mooij J E 2009 Tuning the Gap of a Superconducting Flux Qubit *Phys. Rev. Lett.* **102** 090501
- [3] Fedorov A, Feofanov A K, Macha P, Forn-Díaz P, Harmans C J P M and Mooij J E 2010 Strong Coupling of a Quantum Oscillator to a Flux Qubit at Its Symmetry Point *Phys. Rev. Lett.* **105** 060503
- [4] Fedorov A, Macha P, Feofanov A K, Harmans C J P M and Mooij J E 2011 Tuned Transition from Quantum to Classical for Macroscopic Quantum States *Phys. Rev. Lett.* **106** 170404
- [5] Schwarz M J, Goetz J, Jiang Z, Niemczyk T, Deppe F, Marx A and Gross R 2013 Gradiometric flux qubits with a tunable gap *New J. Phys.* **15** 045001
- [6] Wang X, Miranowicz A, Li H-R and Nori F 2017 Observing pure effects of counter-rotating terms without ultrastrong coupling: A single photon can simultaneously excite two qubits *Phys. Rev. A* **96**, 063820
- [7] Wang X, Miranowicz A, Nori F 2019 Ideal quantum nondemolition readout without Purcell limitations *Phys. Rev. Applied* **12** 064037
- [8] Orlando T P, Mooij J E, Tian L, van der Wal C H, Levitov L S, Lloyd S and Mazo J J 1999 Superconducting persistent-current qubit *Phys. Rev. B* **60** 15398
- [9] Clarke J and Wilhelm F K 2008 Superconducting quantum bits *Nature* **453** 1031
- [10] Yan F et al. 2016 The flux qubit revisited to enhance coherence and reproducibility *Nature Comm.* **7** 12964
- [11] Kim M D, Moon K 2011 Strong coupling of a cavity QED architecture for a current-biased flux qubit *J. Korean Phys. Soc.* **58** 1599; arXiv:1005.1703
- [12] Steffen M, Kumar S, DiVincenzo D P, Rozen J R, Keefe G A, Rothwell M B, Ketchen M B 2010 High-coherence hybrid superconducting qubit *Phys. Rev. Lett.* **105** 100502

- [13] Inomata K, Yamamoto T, Billangeon P-M, Nakamura Y, Tsai J S 2012 Large dispersive shift of cavity resonance induced by a superconducting flux qubit in the straddling regime *Phys. Rev. B* **86** 140508(R)
- [14] Inomata K, Koshino K, Lin Z R, Oliver W D, Tsai J S, Nakamura Y and Yamamoto T 2014 Microwave Down-Conversion with an Impedance-Matched System in Driven Circuit QED *Phys. Rev. Lett.* **113** 063604
- [15] Zagoskin A M, Chipouline A, Il'ichev E, Johansson J R and Nori F 2015 Toroidal qubits: naturally-decoupled quiet artificial atoms *Sci. Rep.* **5** 16934
- [16] Kim M D 2015 Ultrastrong coupling in a scalable design for circuit QED with superconducting qubits *Quantum Inf. Process.* **14** 3677
- [17] Kim M D, Kim J 2017 Circuit-QED lattice with circulator *Quantum Inf. Process.* **16** 192
- [18] Chow J M, Corcoles A D, Gambetta J M, Rigetti C, Johnson B R, Smolin J A, Rozen J R, Keefe G A, Rothwell M B, Ketchen M B, Steffen M 2011 Simple all-microwave entangling gate for fixed-frequency superconducting qubits *Phys. Rev. Lett.* **107** 080502
- [19] Strand J D, Ware M, Beaudoin F, Ohki T A, Johnson B R, Blais A and Plourde B L T 2013 First-order sideband transitions with flux-driven asymmetric transmon qubits *Phys. Rev. B* **87** 220505(R)
- [20] Baust A, Hoffmann E, Haeberlein M, Schwarz M J, Eder P, Goetz J, Wulschner F, Xie E, Zhong L, Quijandría F, Peropadre B, Zueco D, Ripoll J-J G, Solano E, Fedorov K, Menzel E P, Deppe F, Marx A and Gross R 2015 Tunable and switchable coupling between two superconducting resonators *Phys. Rev. B* **91** 014515
- [21] Baust A, Hoffmann E, Haeberlein M, Schwarz M J, Eder P, Goetz J, Wulschner F, Xie E, Zhong L, Quijandría F, Zueco D, Ripoll J-J G, García-Álvarez L, Romero G, Solano E, Fedorov K G, Menzel E P, Deppe F, Marx A and Gross R 2016 Ultrastrong coupling in two-resonator circuit QED *Phys. Rev. B* **93** 214501
- [22] Wulschner et al. 2016 Tunable coupling of transmission-line microwave resonators mediated by an rf SQUID *EPJ Quantum Technol* **3** 10
- [23] Lindstrom T, Webster C H, Healey J E, Colclough M S, Muirhead C M, Tzalenchuk A Y 2007 Circuit QED with a flux qubit strongly coupled to a coplanar transmission line resonator *Supercond. Sci. Technol.* **20** 814
- [24] Oelsner G, van der Ploeg S H W, Macha P, Hubner U, Born D, Anders S, Il'ichev E, Meyer H-G, Grajcar M, Wünsch S, Siegel M, Omelyanchouk A N, Astafiev O 2010 Weak continuous monitoring of a flux qubit using coplanar waveguide resonator *Phys. Rev. B* **81** 172505
- [25] Tinkham M 1996 *Introduction to Superconductivity* (New York: McGraw-Hill)
- [26] Kim M D 2021 Circulator function in a Josephson junction circuit and braiding of Majorana zero modes *Sci. Rep.* **11** 1826
- [27] Kim M D and Hong J 2004 Coupling of Josephson current qubits using a connecting loop *Phys. Rev. B* **70** 184525
- [28] Meservey R and Tedrow P M 1969 Measurements of the kinetic inductance of superconducting linear structures *Journal of Applied Physics* **40** 2028
- [29] Hazard T M, Gyenis A, Di Paolo A, Asfaw A T, Lyon S A, Blais A and Houck A A 2019 Nanowire superinductance fluxonium qubit *Phys. Rev. Lett.* **122** 010504
- [30] Chen Z et al. 2014 Fabrication and characterization of aluminum airbridges for superconducting microwave circuits *Appl. Phys. Lett.* **104** 052602
- [31] Dunsworth A et al. 2018 A method for building low loss multi-layer wiring for superconducting microwave devices *Appl. Phys. Lett.* **112** 063502
- [32] Abuwasib M, Krantz P and Delsing P 2013 Fabrication of large dimension aluminum air-bridges for superconducting quantum circuits *J. Vac. Sci. Technol. B* **31** 031601
- [33] Kim M D, Shin D and Hong J 2003 Double-well potentials in current qubits *Phys. Rev. B* **68** 134513
- [34] van der Wal C H, ter Haar A C J, Wilhelm F K, Schouten R N, Harmans C J P M, Orlando T

- P, Lloyd S and Mooij J E 2000 Quantum superposition of macroscopic persistent-current states *Science* **290** 773
- [35] Blais A, Huang R-S, Wallraff A, Girvin S M and Schoelkopf R J 2004 Cavity quantum electrodynamics for superconducting electrical circuits: An architecture for quantum computation *Phys. Rev. A* **69** 062320
- [36] Blais A, Gambetta J, Wallraff A, Schuster D I, Girvin S M, Devoret M H and Schoelkopf R J 2007 Quantum-information processing with circuit quantum electrodynamics *Phys. Rev. A* **75** 032329